RSC Advances

ROYAL SOCIETY OF CHEMISTRY

www.rsc.org/advances

Journal Name

ARTICLE

A CuO-ZnO Nanostructured p-n Junction Sensor for Enhanced N-butanol Detection†

Yalu Chen, Zhurui Shen*, Qianqian Jia, Jiang Zhao, Zhe Zhao, Huiming Ji*

Received 00th January 20xx,
Accepted 00th January 20xx

DOI: 10.1039/x0xx00000x
www.rsc.org/

Herein, a novel CuO-ZnO nanostructured p-n junction composite is prepared via the hydrothermal method. It is composed of ZnO two dimensional (2-D) porous nanosheets assembly and leaf-like 2-D CuO nanoplates. Then, its gas sensing performance toward n-butanol is studied here. The 2-D/2-D CuO-ZnO composite sensor shows 2.7 times higher sensitivity than that of pure ZnO at 220 ℃. Moreover, its response to n-butanol is 3.5~84 times higher than those for other target gases. This reveals an excellent selectivity toward n-butanol. Its detection limit for n-butanol is calculated to be 0.4 ppm, indicating a potential advantage in low concentration detection. The significant enhancement of composite in sensing performance can be firstly attributed to the p-n junction, which brings the electronic sensitization for the composite sensor. Moreover, the porous structure and the open 2-D/2-D heterostructure also contribute to the sensing performance of the composite. These allow the gas molecules diffuse rapidly, making the chemisorption and the surface reactions on the p-n junction more easily.

1.Introduction

Semiconductor gas sensors have been widely studied due to their important applications in environmental monitoring and medical diagnosis[1-3]. Zinc oxide (ZnO, n-type, band gap: 3.37 eV) exhibits excellent sensing performance toward various oxidizing and reducing gases. It also has advantages of low cost, simplicity in fabrication, and miniaturization[4-6]. Therefore, many reports have focused on improving its gas sensing performance[7-9]. These mainly include morphology modification[6, 10-12], exposing certain crystal facet[13-15], and surface decoration[16-18] etc.

Recently, combining ZnO with p-type semiconductor has attracted great attention due to its enhanced sensing performance[19-25]. By fabricating a p-n junction, charge transfer will occur to equalize the Fermi level, resulting in changes of energy structure of ZnO[19, 26]. Moreover, certain metal oxide (e.g. CuO[27], NiO[28] and Cr_2O_3[29]) can also promote the surface catalytic decomposition of some target gases. Thus electronic sensitization could be simultaneously induced by the formation of p-n junction[19, 21, 26, 30]. This can contribute to the improved sensitivity, selectivity and operating temperature. Up to date, many ZnO based p-n junction sensors have been fabricated in recent years, such as CuO-ZnO[19-21], NiO-ZnO[24] and Cr_2O_3-ZnO[22, 23, 25]*et al*. Amongst, CuO-ZnO heterostructures have attracted growing interest. They always have low detection limits[19, 21, 30, 31] and enhanced selectivity[32-34]. Thus, many efforts have been paid on their morphology design to further improve their sensing performance. For example, Xie *et al.*[21] have prepared three-dimensional (3D) ordered CuO-ZnO inverse opals using polymethylmethacrylate (PMMA) template. Its corresponding sensor achieved a very low detection limit toward acetone as 100 ppb. Zhang *et al.*[19] have synthesized flower-like CuO-ZnO heterojunction nanorods via a co-precipitation method. This CuO-ZnO nanorod sensor exhibited much better selectivity toward ethanol than that of pure ZnO sample. In summary, successful examples of different topological structures can be listed as follow: 0-D/0-D[21, 31, 33], 0-D/1-D[32, 34, 35], 1-D/1-D[18], 2-D/1-D[35, 36], 0-D/3-D[19]and 3-D/3-D[37](n-D represents for n-dimensional structure)etc. However, the synthesis of 2-D/2-D CuO-ZnO heterostructures is rarely reported. It is known that 2-D nanomaterials have attracted great attention due to their large surface to volume ratio, special electronic properties and abundant surface active sites[38-41]. As gas sensing is mainly based on the surface chemical reactions, these advantages would greatly improve the sensitivity of sensor. Therefore, it would be interesting to combine two 2-D semiconductors into a p-n junction. This novel topological design would bring some benefits for gas sensing.

Key Laboratory of Advanced Ceramics and Machining Technology, Ministry of Education, School of Materials Science and Engineering, Tianjin University, Tianjin 300072, PR China, *E-mail:shenzhurui@tju.edu.cn; jihuiming@tju.edu.cn.
†Electronic Supplementary Information (ESI) available.
SeeDOI: 10.1039/x0xx00000x

Herein, a novel p-n junction sensor composed of 2-D ZnO porous nanosheets assembly and 2-D CuO leaf-like nanoflakes have been fabricated. Its gas sensing performance toward n-butanol is studied. N-butanol is mainly used as the raw material for organic agents production[42] and the industrial solvent[43-45]. Besides, n-butanol has the advantages of a high energy content, being less hydroscopic and less corrosive[45]. Thus it is a promising gasoline substitute[42, 45].However, n-butanol vapor is inflammable, explosive and could cause symptoms such as dizziness, headache somnolence and dermatitis[44]. In this work, the sensor response toward 100 ppm n-butanol is 174.3 at 220 °C. Its theoretical detection limit is estimated to 0.4 ppm. Also, the 2-D/2-D CuO-ZnO p-n junction sensor exhibits much better n-butanol selectivity than that of pure ZnO sensor. The possible gas sensing mechanism of CuO-ZnO p-n junction sensor is discussed afterwards. This finding will be useful for the design of metal oxides heterostructures for application in gas sensing.

2.Experimental

2.1 Preparation of porous ZnO microspheres

All chemical reagents were analytical grade and were used as received. In a typical procedure, 0.5 mmol $Zn(NO_3)_2$•$6H_2O$, 2 mmol L-Glutamine and 0.5 mmol $NaCO_3$•$10H_2O$ were dissolved in 20 ml of distilled water. Then, the mixture was transferred into 25 mL Teflon-lined stainless autoclave and maintained at 140 ^oC for 12 h. The autoclave was cooled to room temperature naturally, and the obtained $Zn_5(CO_3)_2(OH)_6$ precipitate was washed with distilled water and ethanol before being dried in air at 80 °C. Finally, the porous ZnO microspheres were obtained after annealing the $Zn_5(CO_3)_2(OH)_6$ precipitate at 400 ^oC for 2 h in air.

2.2 Preparation of CuO-ZnO composite

Briefly, 0.04 g porous ZnO microspheres were dispersed in 20 ml $Cu(NO_3)_2$ solution and stirred for 0.5 h. The weight ratio of CuO/ZnO was 1/10. Afterward, the mixture was transferred into Teflon-lined stainless autoclave and maintained at 120 ^oC for 1.5 h, respectively. After the autoclave cooled to room temperature, the obtained precipitate was washed with distilled water/ethanol and dried in air at 80 °C.

2.3 Characterization

The crystalline structures of the porous ZnO microspheres and CuO-ZnO composite were examined by X-ray diffraction instrument (XRD, Rigaku D/max 2500 diffractometer at 40 kV and 200 mA with Cu Kα radiation). The morphological features and element composition of the samples were investigated by field emission scanning electron microscopy (SEM, Hitachi Model S-4800), energy dispersive spectrometry (EDS), transmission electron microscopy, and high-resolution transmission electron microscopy (TEM, HR-TEM, FEI Tecnai G2 F20). The specific surface area test was performed using a NOVA 2200e surface area analyzer.

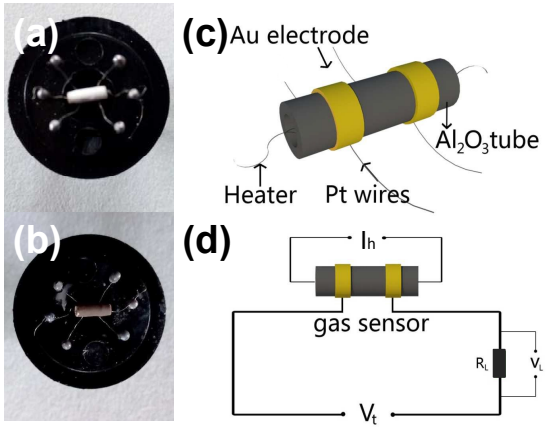

Fig. 1. (a) Digital photo of ZnO sensor, (b) digital photo of CuO-ZnO composite sensor, (c) schematic diagram of a typical gas sensor and (d) measuring electric circuit of gas sensing properties.

2.4 Fabrication and measurement of gas sensor

Fig. 1 (a) and (b) display digital photos of ZnO and CuO-ZnO composite sensors, and (c) displays the schematic diagram of a typical gas sensor. The preparation and measurement of the side-heating sensor are similar to those depicted in our previous report[6, 46]. A proper amount of porous ZnO microspheres or CuO-ZnO composite powders were mixed with several drops of distilled water to form a paste, which was then coated onto the Al_2O_3 tube posited with a pair of Au electrodes and four Pt wires. A Ni–Cr alloy filament which was inserted into the tube was used as heater, and the temperature of coated tube was controlled by regulating the heating current. As displays in Fig. 1 (d), the gas sensing properties were measured by a CGS-8 intelligent gas sensing analysis system (Beijing Elite Tech Co. Ltd., China). A heating current (I_h) range from 0 to 300 mA was applied, and a test voltage (V_t) was supplied to the sensor. A load resistor R_L was connected to the sensor, whose resistance was measured and used for calculating and outputting the sensor resistance. The sensor response was defined as S=Ra/Rg, where Ra and Rg were the resistance of the sensor in air and in target gas, respectively. The gas sensor was aged completely for hours at the optimum working temperature before measurement to improve the mechanical strength and electrical contact, and to ensure its stability and repeatability.

3.Results and discussion

3.1 Composition and morphology

XRD pattern of precipitate obtained during the first hydrothermal process is displayed in Fig. S1. This XRD pattern indicates that the as-prepared precipitate has low crystallinity and all diffraction peaks can be indexed with $Zn_5(CO_3)_2(OH)_6$ standard card (JCPDS No. 19-1458). Fig. 2 compares the XRD

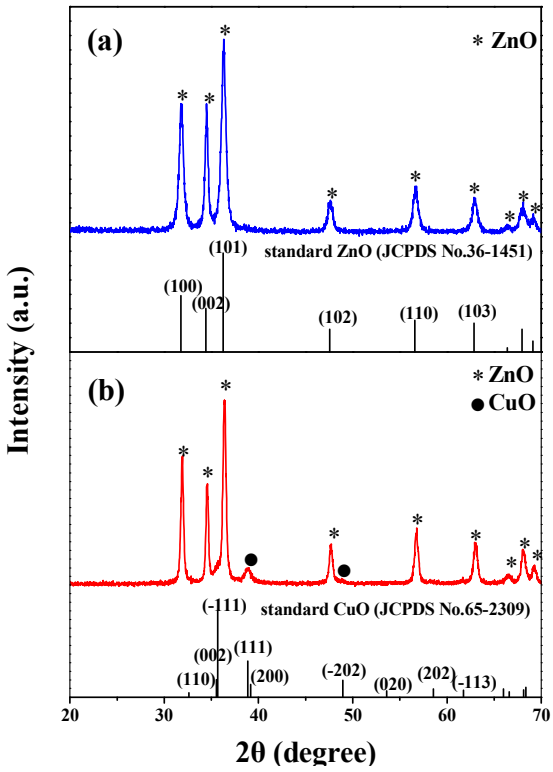

Fig. 2. XRD patterns of (a) as-prepared ZnO and (b) CuO-ZnO composite.

pattern of as-prepared ZnO and CuO-ZnO composite. XRD pattern of as-prepared ZnO (Fig. 2(a)) is well indexed with standard card of hexagonal wurtzite ZnO (JCPDS No. 36-1451). No impurities can be found in this pattern. XRD pattern of CuO-ZnO composite (Fig. 2(b)) displays the characteristic of both wurtzite ZnO and CuO (JCPDS No. 65-2309), and no other peak related to impurities is observed. The XRD pattern of CuO-ZnO composite exhibits two main peaks of monoclinic CuO located at 38.8 and 48.9 degree corresponding to (111) and (-202) planes, respectively. The broad and weak diffraction peaks indicate the small grain size and poor crystallinity of CuO.

SEM images of $Zn_5(CO_3)_2(OH)_6$ precipitate are displayed in Fig. 3(a) and (c). Spherical hierarchical structures of $Zn_5(CO_3)_2(OH)_6$ precipitate are uniformly distributed with the size of 8~12 μm approximately. They are self-assembled by numerous nanosheets, whose thickness is about 20 nm and surface is smooth. As shown in Fig. 3(b) and (d), ZnO exhibits similar shape with $Zn_5(CO_3)_2(OH)_6$ microspheres, but the nanosheets are porous after annealing. Fig. 3(e) shows a low magnification TEM image of ZnO microspheres, demonstrating the characteristic of solid core and saw-tooth like edge. High magnification TEM image of a single ZnO nanosheet (Fig. 3(f)) also displays the porous structure of the nanosheet with the pore size of 10~50 nm. These pores may originate from the decomposition of $Zn_5(CO_3)_2(OH)_6$ during the calcination process[47-50].During the heat treatment a great amount of gases such as CO_2 and H_2O volatilized from the nanosheets, the decomposition reaction can be expressed as Eqs. (1)[49, 50]and numerous vacancies remained. Then, the pores were formed within the nanosheets, as those vacancies were condensed into pores following the Kirkendall effects[49].

$$Zn_5(CO_3)_2(OH)_6 \rightarrow 5\ ZnO + 3\ H_2O + 2\ CO_2 \qquad (1)$$

The HRTEM image (Fig. 3(g)) displays clear lattice fringes with the *d*-spacing of 0.26 nm, corresponding to the (0001) facet of wurtzite ZnO. Moreover, the SAED pattern depicts the well-defined single crystal of ZnO nanosheet and can be indexed to the $[0\bar{1}10]$ zone axis of wurtzite ZnO (Fig. 3(g), inset).

Fig. 4(a) and (b) display low magnification SEM images of ZnO porous microsphere and CuO-ZnO composite, respectively, and (c) displays high magnification SEM image of CuO-ZnO composite. By comparing Fig. 4(a), (b) and (c), it

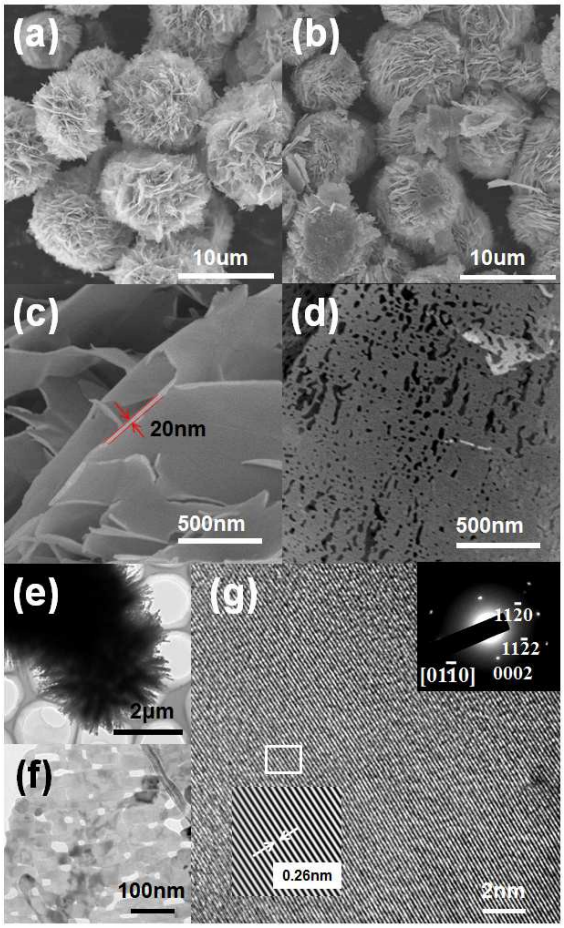

Fig. 3. (a, c) SEM images of as-prepared $Zn_5(CO_3)_2(OH)_6$ precipitate, (b, d) SEM images, (e, f) TEM images, (g) HRTEM image and SAED pattern (inset) of as-prepared ZnO.

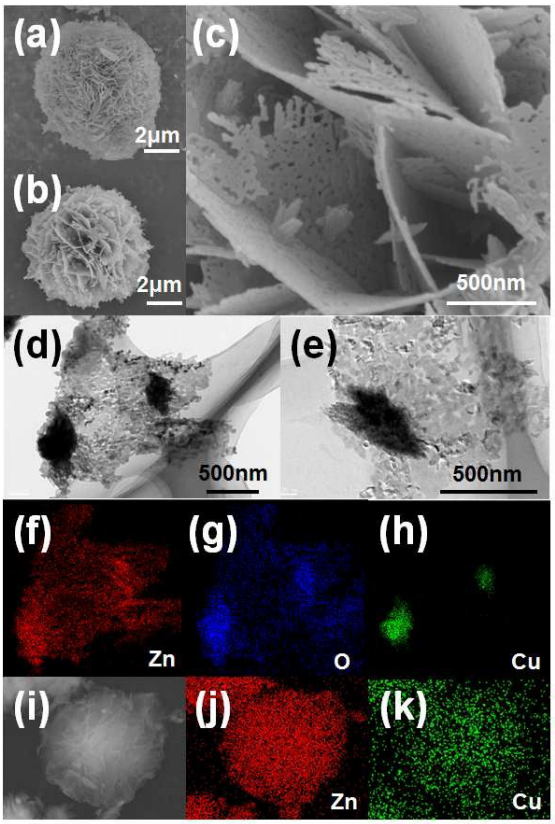

Fig. 4. (a) SEM image of ZnO porous microsphere, (b, c) SEM images, (d-e) TEM images and (f-h) corresponding elemental mapping images, (i-k) SEM image and corresponding elemental mapping images of CuO-ZnO composite.

can be seen that after the second hydrothermal process, the hierarchical structure and porous nanosheets of ZnO microsphere are maintained, and leaf-like structures grow outward on the surface of ZnO nanosheets. Fig. 4(d) and (e) also demonstrate that there are dark leaf-like structures with the length of about 500 nm attached on ZnO nanosheet. In order to clarify the composition of the leaf-like structures, TEM elemental mapping was performed. As shown in Fig. 4(f)-(h), the signals of Cu are concentrated on the dark leaf-like areas in Fig. 4(d), and the signals of O are also enriched in these areas. Considering the result of XRD pattern of CuO-ZnO composite, the leaf-like structures can be confirmed as CuO. EDS mapping is conducted to clearly confirm the spatial distribution of leaf-like CuO in the hierarchical composite microsphere. As shown in Fig. 4(i)-(k), the signals of Zn and Cu are detected uniformly in the whole sphere region, indicating the uniform distribution of leaf-like CuO on ZnO microsphere. Growth mechanism of the obtained nanostructures is discussed and details see Section S1.

Herein, to study the chemical nature and the surface related sensing mechanism, XPS analysis was performed for ZnO and CuO-ZnO (Fig. S8, Table S1). Fig. S8a shows that the Zn 2p spectra of ZnO and CuO-ZnO were similar for their energy positions and distribution. As shown in Fig. S8b, the Cu 2p spectrum of CuO-ZnO showed a characteristic of CuO[51], the calculated Cu: Zn ratio is 1: 8.4. This indicates a 10.6 % molar ratio of CuO in the composite. While there was no obvious Cu 2p signal for the pure ZnO.

3.2 Gas-sensing performance

Working temperature is an important indicator for a gas sensor. It is closely related to energy consumption, easy usage, testing convenience, etc.[52] For semiconductor gas sensors, working temperature can greatly affect the kinetics of gas sensing. This include molecules chemisorption, desorption and chemical reactions on the surface of sensing materials[6, 8]. During gas sensing process, these factors will reach a balance, and exhibits the best response at optimum working

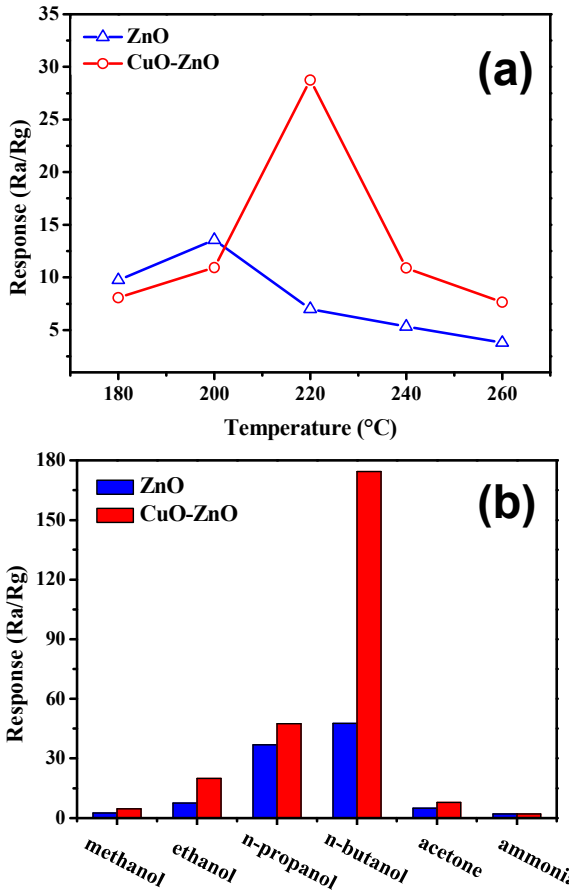

Fig. 5. (a) Sensing response of ZnO and CuO-ZnO composite sensors toward 20 ppm n-butanol at different working temperatures, (b) response of ZnO and CuO-ZnO composite sensors to various 100 ppm VOC gases at 200 °C and 220 °C, respectively.

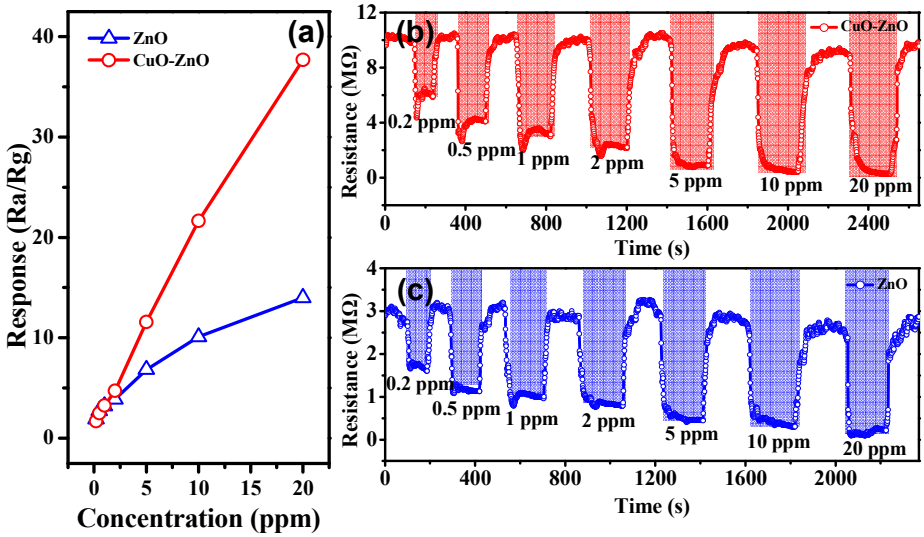

Fig. 6. (a) Sensing response and (b, c) transient curve of CuO-ZnO composite and ZnOsensors toward different concentration of n-butanol.

temperature[13, 52-54]. In this study, response of ZnO and CuO-ZnO composite sensors toward 20 ppm n-butanol at different working temperatures were tested, as displayed in Fig. 5(a). It is depicted that the response value increases firstly with increasing working temperature and then decreases. The maximum responses of ZnO and CuO-ZnO sensors are reached at an optimum working temperature of 200°C and 220 °C, respectively. This working temperature is relatively low compared with other ZnO-based materials[55-58]. The responses of ZnO and CuO-ZnO sensors to 100 ppm of various VOC gases (methanol, ethanol, n-propanol, n-butanol, acetone and ammonia) were measured at 200 °C and 220 °C, respectively, as shown in Fig. 5(b). Obviously, CuO-ZnO composite sensor shows enhanced response to most of the test gases than the sensor based on pure ZnO microspheres. Moreover, the response of CuO-ZnO composite sensor to n-butanol is 3.5-84 times higher than those toward other testing gases, revealing an enhanced and excellent selectivity toward n-butanol.

The responses of ZnO and CuO-ZnO composite sensors toward different concentration of n-butanol were measured at 200 °C and 220 °C, respectively, as shown in Fig. 6 (a)-(c). The resistance of CuO-ZnO composite sensor in air (about 10 MΩ) is obviously higher than that of ZnO sensor (about 3 MΩ). Besides, the resistivity was tested by Hall measurement (HALL-8800, details are shown in Fig.S9).The resistivity of ZnO and CuO-ZnO is 0.716E+3 Ω·cm and 1.254E+3 Ω·cm, respectively, which are consistent with the resistance of the ZnO and CuO-ZnO sensors in air. As p-n junction can lead to band barrier and wide depletion layers, this resistivity increase could prove the formation of CuO-ZnO p-n junctions[26, 29, 59].The resistance of the two sensors decrease after inducing n-butanol, exhibiting n-type semiconductor characteristic. The sensing responses of ZnO and CuO-ZnO composite sensors are calculated and displayed in Fig. 6(a). It can be seen that CuO-ZnO composite sensor exhibits much higher response than ZnO sensor. The sensing response of CuO-ZnO composite sensor to 20 ppm n-butanol is 37.7, which is about 2.7 times of ZnO

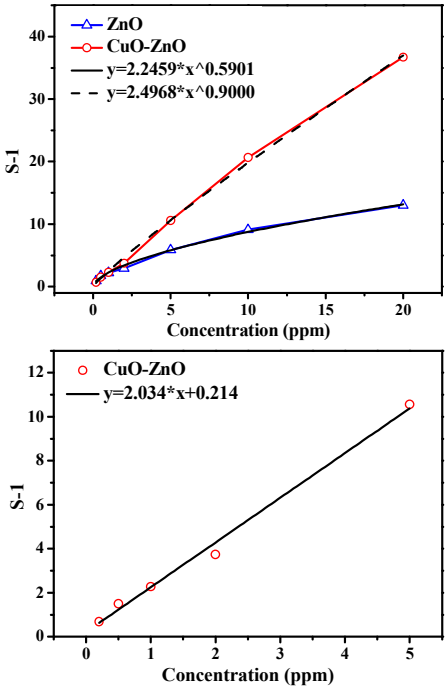

Fig. 7. (a) Plot of power function fitting and (b) linear fitting of S-1 versus concentration of n-butanol.

Table 1 Gas sensing properties toward n-butanol in present study and other literatures.

Sensing materials	Working temperature (°C)	Concentration (ppm)	Response	Reference
Au/ ZnO microsheets	240	20	18.5	[16]
Au NPs-ZnO NWs	320	100	18.2	[60]
ZnO microflowers	320	100	24.1	[10]
3D flower-like ZnO nanostructures	220	100	49	[11]
ZnO nanoparticles	320	100	62	[61]
$ZnFe_2O_4$/ZnO nanoheterostructure	260	200	26	[62]
$ZnFe_2O_4$/ZnO hollow microsphere	320	200	27.7	[63]
ZnO@ZnS core/shell microrods	300	500	48.5	[64]
ZnO nanoflakes	330	500	87	[13]
ZnO porous microspheres	200	20 100	14 47.5	This work
CuO-ZnO composite	220	20 100	37.7 174.3	This work

sensors' response. In comparison with previous studies, CuO-ZnO composite sensor exhibits considerably enhanced sensitivity toward n-butanol than other ZnO based sensing materials. In addition, both ZnO and CuO-ZnO composite sensors exhibit excellent response and recovery characteristics with respect to different concentration of n-butanol. The responses of both sensors are fast and significant even to 0.5 ppm n-butanol. Meanwhile, the sensors' resistance could basically return to the baseline every cycle after inducing the air. Thus, both of the sensor are stable enough to enable the practically repeatable detection of low concentrations of n-butanol.

The response of metal oxide semiconductor gas sensor can usually empirically represented as $S-1=\alpha[C]^{\beta}$[14, 44, 65]. Herein, S is the response value of the sensor, C is the concentration of target gas, α is a parameter and β is the surface charge parameter with value from 0.5 to 1[14]. Fig. 7(a) displays the plot of S-1 versus C of ZnO and CuO-ZnO composite sensors, where a power function relationship as described by above equation is observed. The values of β of ZnO and CuO-ZnO composite sensors are 0.59 and 0.90, respectively. The value of β is depending on the charge of the surface species and the stoichiometry of the elementary reactions on the surface[14, 65, 66]. Thus, the difference between the values of β indicating that the gas sensing mechanism of these two samples may be different. As shown in Fig. 7(b), the response of CuO-ZnO composite sensor has a good linear relationship (R=0.9913) with the concentration of n-butanol in the range of 0.2-5 ppm. Thus, the theoretical detection limit (DL) as defined in article [67] can be calculated to be 0.4 ppm, which is a relatively low detection limit for n-butanol.

3.3 Gas sensing mechanism

Generally, gas sensing behavior of ZnO is resulted from the surface chemical reactions. The reactants are the chemisorbed oxygen species (O^-, O^{2-} and O_2^-) and the adsorbed target gas molecules. These reactions lead to the resistance variation of the gas sensor. High specific surface area of sensing material usually has positive effects on the sensing response[52]. Thus the specific surface area test was performed, and the nitrogen adsorption–desorption isotherms are provided in Fig. S10. The specific surface area of CuO-ZnO composite is 46 m^2/g which is not significantly larger than that of ZnO porous microspheres (35 m^2/g). Their difference of surface area is not the main factor for their difference in sensing response. Therefore, the higher sensitivity of CuO-ZnO composite could be attributed to the electronic sensitization induced by CuO[68, 69]. There are more active sites[69] and more chemisorbed oxygen species on the surface of p-type semiconductors than those of n-type semiconductors[70]. The modified CuO nanostructures could act as a strong acceptor of electrons from ZnO[68].The Fermi energy levels of n-type ZnO and p-type CuO are equalized due to the charge transfer, as shown in Fig. S11[71, 72]. Moreover, as shown in the Mott-Schottky curve (Fig.S12.), CuO-ZnO composite exhibits smaller slope than the ZnO, indicating that the introduction of CuO increases the carrier density of the ZnO. Besides, the flat band potential of the ZnO is shift positively by about 0.2 V

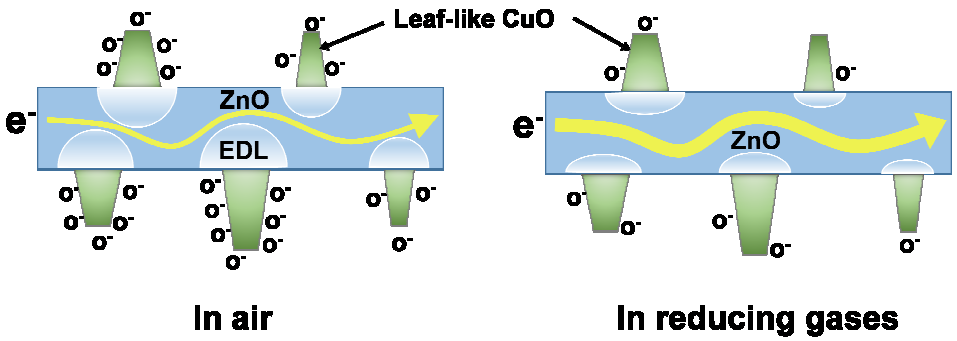

Fig. 8. Illustration of sensing mechanism for CuO-ZnO p-n junction toward reducing gases.

after the addition of the CuO. These results suggest the electron redistribution between the ZnO and the CuO[73]. In the air, oxygen molecules capture electrons from CuO, and chemisorbed oxygen species are formed on its surface[74]. Meanwhile, electrons transfer from ZnO to CuO, causing the formation of an electrons depletion layer (EDL) extending into ZnO[69]. The formation of EDL would significantly narrow the conducting part and dominate the conductivity of CuO-ZnO[29, 59].Upon exposure to reducing gases, the gas molecules react with chemisorbed oxygen and electrons are released to CuO. Then, the electrons return to ZnO, leading to the reduction of EDL thickness and the increase of conductivity of CuO-ZnO. The illustration of sensing mechanism for CuO-ZnO p-n junction toward reducing gases is shown in Fig.8. Compared to pure ZnO, the decoration of CuO promotes the chemisorption of oxygen species and the chemical reactions on the surface of CuO-ZnO[19, 69].This leads to an enhancement in sensitivity of composite. Moreover, the quantity of chemisorbed oxygen species can be evaluated by the intensity of Oc component in the O 1s XPS specra[14, 75, 76]. As shown in Table S1, the relative percentage of O_C component of CuO-ZnO is 18.7 % which is higher than ZnO (12.7 %). This result could further prove the sensing mechanism of CuO-ZnO p-n junction.

In addition, the porous hierarchical structure of ZnO and the 2D-2D topology also contribute to the excellent gas sensing performance. The porous hierarchical structure of ZnO provides channels for diffusion of gas molecules[6, 77].Moreover, it also provides more active sites and improves the kinetics of chemical reactions on the surface[77].This also results in enhanced sensing performance. Furthermore, there would be more oxygen species chemisorbed on the surface of 2D CuO than 0D and 1D structures due to its large surface to volume ratio[78]. Thus the sensitivity of the CuO-ZnO composite is further enhanced.

4.Conclusion

In summary, a CuO-ZnO p-n junction composite with the2-D/2-D topology has been synthesized. Then, the gas sensing performance of CuO-ZnO composite and pure ZnO toward n-butanol is studied. The CuO-ZnO composite sensor shows 2.7 times higher sensitivity than that of pure ZnO at 220 °C. Moreover, CuO-ZnO composite sensor exhibits a better selectivity toward n-butanol than that of pure ZnO. The enhanced sensing performance of composite can be attributed to the p-n junction at first. The introduction of CuO brings both the electronic sensitization for the composite sensor. This results in the significant enhancement in sensitivity. Moreover, the enhancement in sensitivity can also be attributed to the porous nanostructure and the open 2-D/2-D heterostructure. This structure allows the target gas molecules diffuse rapidly, making the chemisorption and the chemical reactions on the p-n junctions more easily.

Acknowledgements

This work was supported by the National Natural Science Foundation of China (Grant nos. 51172157, 21303118) and the Specialized Research Fund for the Doctoral Program of Higher Education (No. 20130032120003) and the Seed Foundation of Tianjin University.

Notes and references

1. L. Wang, A. Teleki, S. Pratsinis and P. Gouma, *Chemistry of Materials*, 2008, **20**, 4794-4796.
2. S. Deng, V. Tjoa, H. M. Fan, H. R. Tan, D. C. Sayle, M. Olivo, S. Mhaisalkar, J. Wei and C. H. Sow, *Journal Of the American Chemical Society*, 2012, **134**, 4905-4917.
3. J. Reichel, T. Seyffarth, U. Guth, H. Möbius and D. Göckeritz, *Die Pharmazie*, 1989, **44**, 698-702.
4. A. Raju and C. Rao, *Sensors and Actuators B: Chemical*, 1991, **3**, 305-310.
5. X. Wu, K. Li and H. Wang, *Journal Of Hazardous Materials*, 2010, **174**, 573-580.
6. Q. Q. Jia, H. M. Ji, Y. Zhang, Y. L. Chen, X. H. Sun and Z. G. Jin, *Journal Of Hazardous Materials*, 2014, **276**, 262-270.
7. M. Chen, Z. Wang, D. Han, F. Gu and G. Guo, *Sensors And Actuators B-Chemical*, 2011, **157**, 565-574.

8. S. L. Bai, T. Guo, Y. B. Zhao, R. X. Luo, D. Q. Li, A. F. Chen and C. C. Liu, *J. Mater. Chem. A*, 2013, **1**, 11335-11342.
9. X. Zhou, W. Peng, C. Wang, X. L. Hu, X. W. Li, P. Sun, K. Shimanoe, N. Yamazoe and G. Y. Lu, *J. Mater. Chem. A*, 2014, **2**, 17683-17690.
10. J. Huang, Y. Wu, C. Gu, M. Zhai, K. Yu, M. Yang and J. Liu, *Sensors And Actuators B-Chemical*, 2010, **146**, 206-212.
11. H. Zhang, R. Wu, Z. Chen, G. Liu, Z. Zhang and Z. Jiao, *Crystengcomm*, 2012, **14**, 1775-1782.
12. Z. D. Lin, F. Guo, C. Wang, X. H. Wang, K. Wang and Y. Qu, *RSC Adv.*, 2014, **4**, 5122-5129.
13. Y. V. Kaneti, J. Yue, X. Jiang and A. Yu, *J. Phys. Chem. C*, 2013, **117**, 13153-13162.
14. M. R. Alenezi, A. S. Alshammari, K. Jayawardena, M. J. Beliatis, S. J. Henley and S. R. P. Silva, *J. Phys. Chem. C*, 2013, **117**, 17850-17858.
15. Q. Zhao, Q. Shen, F. Yang, H. Zhao, B. Liu, Q. Liang, A. H. Wei, H. Q. Yang and S. Z. Liu, *Sensors And Actuators B-Chemical*, 2014, **195**, 71-79.
16. L. Wang, S. Wang, H. Zhang, Y. Wang, J. Yang and W. Huang, *New J. Chem.*, 2014, **38**, 2530-2537.
17. C. W. Na, H. S. Woo, I. D. Kim and J. H. Lee, *Chem. Commun.*, 2011, **47**, 5148-5150.
18. P. Rai, S.-H. Jeon, C.-H. Lee, J.-H. Lee and Y.-T. Yu, *RSC Adv.*, 2014, **4**, 23604-23609.
19. Y. B. Zhang, J. Yin, L. Li, L. X. Zhang and L. J. Bie, *Sensors And Actuators B-Chemical*, 2014, **202**, 500-507.
20. T. Y. Tiong, C. F. Dee, A. A. Hamzah, B. Y. Majlis and S. A. Rahman, *Sensors And Actuators B-Chemical*, 2014, **202**, 1322-1332.
21. Y. Xie, R. Xing, Q. Li, L. Xu and H. Song, *Sensors And Actuators B-Chemical*, 2015, **211**, 255-262.
22. W. Wang, Z. Li, W. Zheng, H. Huang, C. Wang and J. Sun, *Sensors and Actuators B-Chemical*, 2010, **143**, 754-758.
23. D. R. Patil and L. A. Patil, *Talanta*, 2009, **77**, 1409-1414.
24. D. Ju, H. Xu, Z. Qiu, J. Guo, J. Zhang and B. Cao, *Sensors and Actuators B-Chemical*, 2014, **200**, 288-296.
25. D. R. Patil, L. A. Patil and P. P. Patil, *Sensors and Actuators B-Chemical*, 2007, **126**, 368-374.
26. D. R. Miller, S. A. Akbar and P. A. Morris, *Sensors And Actuators B-Chemical*, 2014, **204**, 250-272.
27. I.-S. Hwang, J.-K. Choi, S.-J. Kim, K.-Y. Dong, J.-H. Kwon, B.-K. Ju and J.-H. Lee, *Sensors and Actuators B-Chemical*, 2009, **142**, 105-110.
28. H.-R. Kim, K.-I. Choi, K.-M. Kim, I.-D. Kim, G. Cao and J.-H. Lee, *Chem. Commun.*, 2010, **46**, 5061-5063.
29. H.-S. Woo, C. W. Na, I.-D. Kim and J.-H. Lee, *Nanotechnology*, 2012, **23**, 245501.
30. J. Huang, Y. Dai, C. Gu, Y. Sun and J. Liu, *J. Alloy. Compd.*, 2013, **575**, 115-122.
31. S. Mridha and D. Basak, *Semiconductor Science and Technology*, 2006, **21**, 928-932.
32. H. Le Thuy and S. H. Hur, *Physica Status Solidi a-Applications And Materials Science*, 2013, **210**, 1213-1216.
33. Z. Xu, G. Duan, Y. Li, G. Liu, H. Zhang, Z. Dai and W. Cai, *Chemistry-a European Journal*, 2014, **20**, 6040-6046.
34. N. Datta, N. Ramgir, M. Kaur, S. K. Ganapathi, A. K. Debnath, D. K. Aswal and S. K. Gupta, *Sensors and Actuators B-Chemical*, 2012, **166**, 394-401.
35. S. Pal, S. Maiti, U. N. Maiti and K. K. Chattopadhyay, *Crystengcomm*, 2015, **17**, 1464-1476.
36. A. Zainelabdin, G. Amin, S. Zaman, O. Nur, J. Lu, L. Hultman and M. Willander, *J. Mater. Chem.*, 2012, **22**, 11583-11590.
37. Y. Zhu, Y. Wang, L. Song, X. Chen, W. Liu, J. Sun, X. She, Z. Zhong and F. Su, *RSC Adv.*, 2013, **3**, 9794-9802.
38. T. Yu, B. Lim and Y. Xia, *Angewandte Chemie-International Edition*, 2010, **49**, 4484-4487.
39. W. Zeng, H. Zhang and Z. Wang, *Appl. Surf. Sci.*, 2015, **347**, 73-78.
40. M. Choi, K. Na, J. Kim, Y. Sakamoto, O. Terasaki and R. Ryoo, *Nature*, 2009, **461**, 246-U120.
41. X. Zhang and Y. Xie, *Chemical Society Reviews*, 2013, **42**, 8187-8199.
42. L. Yu, M. Xu, I. C. Tang and S.-T. Yang, *Applied Microbiology and Biotechnology*, 2015, **99**, 6155-6165.
43. S. Deng, N. Chen, D. Deng, Y. Li, X. Xing and Y. Wang, *Ceramics International*, 2015, **41**, 11004-11012.
44. H. Wang, Y. Qu, H. Chen, Z. Lin and K. Dai, *Sensors and Actuators B-Chemical*, 2014, **201**, 153-159.
45. C.-L. Cheng, P.-Y. Che, B.-Y. Chen, W.-J. Lee, L.-J. Chien and J.-S. Chang, *Bioresource Technology*, 2012, **113**, 58-64.
46. Y. Zhang, H. M. Ji, Y. L. Chen and X. H. Sun, *J. Mater. Sci.-Mater. Electron.*, 2014, **25**, 573-580.
47. S. Huang, T. Wang and Q. Xiao, *Journal of Physics and Chemistry of Solids*, 2015, **76**, 51-58.
48. H. Wu, Q. Xie, L. An, P. Jin, D.-L. Peng, C. Huang and H. Wan, *Mater. Lett.*, 2015, **139**, 393-396.
49. S. Liu, C. Li, J. Yu and Q. Xiang, *Crystengcomm*, 2011, **13**, 2533-2541.
50. X. Zhou, Z. Hu, Y. Fan, S. Chen, W. Ding and N. Xu, *J. Phys. Chem. C*, 2008, **112**, 11722-11728.
51. D. A. Svintsitskiy, T. Y. Kardash, O. A. Stonkus, E. M. Slavinskaya, A. I. Stadnichenko, S. V. Koscheev, A. P. Chupakhin and A. I. Boronin, *The Journal of Physical Chemistry C*, 2013, **117**, 14588-14599.
52. Q. Q. Jia, H. M. Ji, D. H. Wang, X. Bai, X. H. Sun and Z. G. Jin, *J. Mater. Chem. A*, 2014, **2**, 13602-13611.
53. A. P. Rambu, V. Tiron, V. Nica and N. Iftimie, *Journal Of Applied Physics*, 2013, **113**.
54. J. Luo, S. Y. Ma, F. M. Li, X. B. Li, W. Q. Li, L. Cheng, Y. Z. Mao and D. J. Gz, *Mater. Lett.*, 2014, **121**, 137-140.
55. W. Guo, X. Li, H. Qin and Z. Wang, *Physica E*, 2015, **73**, 163-168.
56. F. Fan, P. Tang, Y. Wang, Y. Feng, A. Chen, R. Luo and D. Li, *Sensors and Actuators B-Chemical*, 2015, **215**, 231-240.
57. X. Li, X. Zhou, Y. Liu, P. Sun, K. Shimanoe, N. Yamazoe and G. Lu, *RSC Adv.*, 2014, **4**, 32538-32543.
58. D. Wang, S. Du, X. Zhou, B. Wang, J. Ma, P. Sun, Y. Sun and G. Lu, *Crystengcomm*, 2013, **15**, 7438-7442.
59. F. Shao, M. Hoffmann, J. Prades, R. Zamani, J. Arbiol, J. Morante, E. Varechkina, M. Rumyantseva, A. Gaskov and I. Giebelhaus, *Sensors and Actuators B: Chemical*, 2013, **181**, 130-135.

60. C. Gu, S. Li, J. Huang, C. Shi and J. Liu, *Sensors And Actuators B-Chemical*, 2013, **177**, 453-459.
61. X. Liu, N. Chen, X. Xing, Y. Li, X. Xiao, Y. Wang and I. Djerdj, *RSC Adv.*, 2015, **5**, 54372-54378.
62. S. Wang, J. Zhang, J. Yang, X. Gao, H. Zhang, Y. Wang and Z. Zhu, *RSC Adv.*, 2015, **5**, 10048-10057.
63. S. Wang, X. Gao, J. Yang, Z. Zhu, H. Zhang and Y. Wang, *RSC Adv.*, 2014, **4**, 57967-57974.
64. W. Zhang, S. Wang, Y. Wang, Z. Zhu, X. Gao, J. Yang and H. X. Zhang, *RSC Adv.*, 2015, **5**, 2620-2629.
65. S. Tian, F. Yang, D. Zeng and C. Xie, *J. Phys. Chem. C*, 2012, **116**, 10586-10591.
66. N. Yamazoe and K. Shimanoe, *Sensors And Actuators B-Chemical*, 2008, **128**, 566-573.
67. J. Li, Y. Lu, Q. Ye, M. Cinke, J. Han and M. Meyyappan, *Nano Letters*, 2003, **3**, 929-933.
68. N. Yamazoe, G. Sakai and K. Shimanoe, *Catalysis Surveys from Asia*, 2003, **7**, 63-75.
69. S. R. Morrison, *Sensors and actuators*, 1987, **12**, 425-440.
70. M. Iwamoto, Y. Yoda, N. Yamazoe and T. Seiyama, *The Journal of Physical Chemistry*, 1978, **82**, 2564-2570.
71. Z. Guo, D. Zhao, Y. Liu, D. Shen, J. Zhang and B. Li, *Applied Physics Letters*, 2008, **93**, 3501.
72. Q. Bao, C. M. Li, L. Liao, H. Yang, W. Wang, C. Ke, Q. Song, H. Bao, T. Yu and K. P. Loh, *Nanotechnology*, 2009, **20**, 065203.
73. Z. Hu, M. Xu, Z. Shen and J. C. Yu, *J. Mater. Chem. A*, 2015, **3**, 14046-14053.
74. H.-J. Kim and J.-H. Lee, *Sensors and Actuators B-Chemical*, 2014, **192**, 607-627.
75. X. G. Han, H. Z. He, Q. Kuang, X. Zhou, X. H. Zhang, T. Xu, Z. X. Xie and L. S. Zheng, *J. Phys. Chem. C*, 2009, **113**, 584-589.
76. Y. V. Kaneti, Z. J. Zhang, J. Yue, Q. M. D. Zakaria, C. Y. Chen, X. C. Jiang and A. B. Yu, *Physical Chemistry Chemical Physics*, 2014, **16**, 11471-11480.
77. X. Gou, G. Wang, J. Park, H. Liu and J. Yang, *Nanotechnology*, 2008, **19**.
78. S. Jiang, Z. Gui, G. Chen, D. Liang and J. Alam, *Acs Applied Materials & Interfaces*, 2015, **7**, 14603-14613.

Graphical Abstract